III-nitride quantum cascade detector grown by metal organic chemical vapor deposition

Yu Song,[1,a)] Rajaram Bhat,[2] Tzu-Yung Huang,[1] Pranav Badami,[1] Chung-En Zah,[2] and Claire Gmachl[1]
[1]*Department of Electrical Engineering, Princeton University, Princeton, New Jersey 08540, USA*
[2]*Corning Incorporated, Corning, New York 14831, USA*

(Received 15 October 2014; accepted 27 October 2014; published online 4 November 2014)

Quantum cascade (QC) detectors in the GaN/$Al_xGa_{1-x}N$ material system grown by metal organic chemical vapor deposition are designed, fabricated, and characterized. Only two material compositions, i.e., GaN as wells and $Al_{0.5}Ga_{0.5}N$ as barriers are used in the active layers. The QC detectors operates around 4 μm, with a peak responsivity of up to $\sim$100 μA/W and a detectivity of up to 10^8 Jones at the background limited infrared performance temperature around 140 K. © *2014 AIP Publishing LLC*. [http://dx.doi.org/10.1063/1.4901220]

As important members of the family of semiconductor intersubband (ISB) photodetectors,[1–5] quantum cascade (QC) detectors utilize engineered quantized states to obtain light absorption and carrier extraction and can thus operate at zero bias.[6–10] Benefiting from this, QC detectors in traditional III-arsenide and III-phosphide materials achieve a wide range of operating wavelengths with intrinsically low noise and low heat load. Furthermore, the study of intersubband light detection[11–15] and QC structures[16–18] in the III-nitride and II-VI material systems have made significant progress. Taking advantage of the high conduction band offsets and shorter scattering lifetimes, photodetectors[19–22] and especially QC detectors[23–26] in the III-nitride material system are shown to work at shorter wavelengths with faster response. Up to now, molecular beam epitaxy (MBE) has been the exclusive growth techniques for III-nitride QC detectors. It is of clear interest to explore the possibility of such detectors grown by metal organic chemical vapor deposition (MOCVD), which is a faster and industrially more favorable growth technique. Furthermore, since most existing III-nitride QC detectors are designed with at least three material compositions combined, i.e., GaN/AlN/$Al_xGa_{1-x}N$, it is of interest to explore the possibility of only two material compositions and suitable design schemes.

In this work, QC detectors with GaN/$Al_{0.5}Ga_{0.5}N$ superlattices grown by MOCVD technique are designed, fabricated, and characterized. Excellent growth quality is achieved with minimal surface roughness. In the QC detector design, $\sim$90 meV energy spacings are engineered between the upper or lower detector state and the adjoining extractor states, respectively, which ensures a high escape probability of 40% and reduces thermal backfilling. A peak responsivity of $\sim$105 μA/W is recorded with a detectivity of up to 10^8 Jones at 140 K. We have also studied the QC detector formed by reversing the layer sequence of the original design, which produces a responsivity of $\sim$35 μA/W and a detectivity of 10^4 Jones.

The material system employed in this study is c-plane MOCVD grown GaN/$Al_xGa_{1-x}N$ on sapphire substrates. The active layers are comprised of GaN quantum wells and $Al_{0.5}Ga_{0.5}N$ barriers. Composite template layers are employed to release the strain and obtain smooth surface morphology, with surface roughness root mean square (rms) below 0.5 nm. The topmost template layer is 1 μm thick $Al_{0.188}Ga_{0.812}N$ matching to average Al concentration in the epilayers above. This layer also serves as the bottom contact layer with a silicon doping level of 1×10^{19} cm^{-3}. Relaxation-free growth is achieved for the whole epitaxial growth. Above the active layers follows a 150 nm thick $Al_{0.188}Ga_{0.812}N$ layer with silicon doping of 1×10^{19} cm^{-3} serving as the top contact layer.

To design the structures, an effective mass model based on k·p theory has been developed.[27–29] Nonparabolicity is taken into account with an energy dependent effective mass. Nonlinear spontaneous and piezoelectric polarization fields are calculated *in-situ*, with dependence on the actual material compositions and the induced strain in each layer. Periodic boundary conditions are adopted in the design.[30,31] The Poisson equation accounting for the electric potential induced by charge re-distribution is calculated together with the Schrödinger equation iteratively. The material parameters used in the calculation can be found in Refs. 31–34.

The QC detector structure studied in this work is plotted in Fig. 1. The absorbing layer is a 12-monolayer (ML) GaN quantum well, with 4-ML $Al_{0.5}Ga_{0.5}N$ barriers on each side as is shown in Fig. 1. Next to the left is a 7-ML GaN quantum well, followed by 6 repeats of 4-ML $Al_{0.5}Ga_{0.5}N$/6-ML GaN as carrier extraction wells. In QC detectors fabricated with traditional non-polar materials, the extraction layer thicknesses need to be adjusted progressively to obtain proper energy offsets of the extractor states.[9] Here, the extractor wells have nominally identical thicknesses, and the proper biasing is provided by the intrinsic polarization fields, facilitating carrier extraction. N-type silicon doping of 1.8×10^{18} cm^{-3} is introduced to the second and third quantum well to the right of the active layer. Placing the dopant ions away from the active well minimizes impurity scattering from the upper detector state back to the lower detector state in the same well. The structure is repeated 40 times, and the

a)yusong@princeton.edu

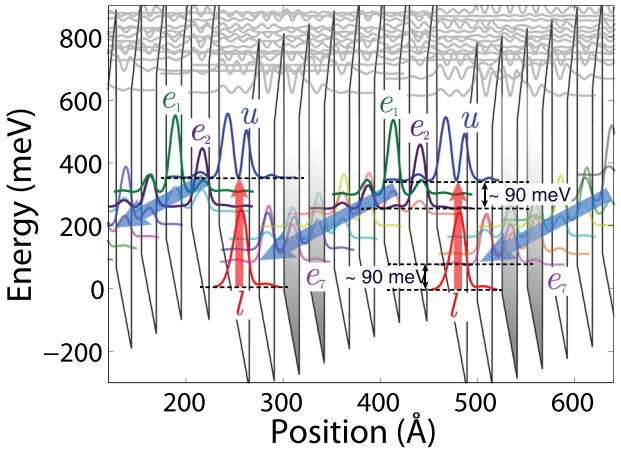

FIG. 1. QC detector design with GaN/$Al_{0.5}Ga_{0.5}N$ superlattices (two periods are shown). The optical transition is indicated with a red arrow. The direction of carrier extraction is indicated with a blue arrow. Designed optical transition is at 3.6 μm with a dipole matrix element of 5.7 Å. The shaded wells are doped to a level of 1.8×10^{18} cm^{-3} with Si. Energy spacings of ~90 meV exist between the states u and e_2, and between l and e_7. Growth direction: left to right.

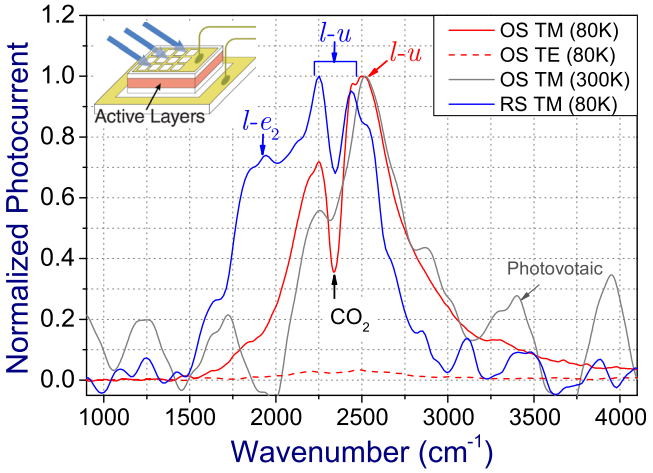

FIG. 2. Normalized photocurrent spectra. Red: TM (solid) and TE (dashed) spectra at 80 K. Grey: TM spectrum at 300 K. Blue: TM spectrum of the reversed structure at 80 K. Inset: Schematic of the fabricated device. Light is incident at the Brewster's angle of 66°. OS and RS refer to the original structure and the reversed structure, respectively.

entire superlattice is sandwiched between the top and bottom contact layers outlined above.

The calculated optical transition wavelength is ~3.6 μm (2780 cm^{-1}); the optical dipole matrix element is 5.7 Å. As is shown in Fig. 1, there are ~90 meV energy spacings between the lower detector state (l) and the adjacent extractor state (e_7), and between the upper detector state (u) and the extractor state centered in the quantum well on the left (e_2). Fast electron extraction is ensured in between these states, since the longitudinal optical phonon (LO) energy is ~91 meV for GaN and ~95 meV for $Al_{0.5}Ga_{0.5}N$. The calculated LO scattering lifetime from u to e_2 is $\tau^{LO}_{u\to e_2} = 0.075$ ps, and that from e_7 to l is $\tau^{LO}_{e_7\to l} = 0.096$ ps. Also the ~90 meV energy spacing before the lower detector state helps preventing backfilling of carriers into the extractor states $\tau^{LO}_{l\to e_7} = 3.1$ ps. Based on the scattering lifetimes, we can estimate the escape probability as $p = \tau_u/\tau_{u\to e_2}$, where τ_u is the upper state lifetime. The estimated $\tau_u = 0.03$ ps considering the major scattering channels from the upper state u to states l, e_7, e_6, e_5 and e_2. Thus, the escape probability is estimated as $p = 40\%$.

Square and round mesas are fabricated as detectors. The mesas were reactive ion etched partly into the bottom contact layer. Contact metallization of Ti 6 nm/Al 180 nm/Ni 55 nm/Au 300 nm is applied by e-beam evaporation. The samples are then annealed at 800°C for 1 min. Ohmic contacts are formed with specific contact resistances of $\leq 5 \times 10^{-4}\,\Omega\,\text{cm}^2$. Then small samples are cut and mounted on copper blocks for measurements. Broadband light is employed for the measurement of the photo response spectra; the light is incident at the Brewster's angle, 66° for this material composition. Square windows are opened in the top contact to let the incident light reach the absorbing layers as shown in the inset of Fig. 2. The detectors are mounted inside cryostats for variable temperature measurements.

The photocurrent response signals are sensed by a lock-in amplifier, and the spectra are recorded by a Fourier Transform Infrared Spectrometer (FTIR). The results are plotted in Fig. 2. A transverse magnetic (TM) over transverse electric (TE) selection ratio of >20 : 1 is recorded (red solid and dashed curves). This is a direct evidence of the ISB origin of the light absorption.[1] The QC detector operates from cryogenic to room temperature. The photovoltage spectrum at 300 K is also plotted in Fig. 1, with no significant difference in peak absorption energy or broadening. The photocurrent spectrum at 80 K is centered at 4 μm (2500 cm^{-1}) with a full width at half maximum (FWHM) of about 640 cm^{-1} (80 meV) from 2110 cm^{-1} to 2750 cm^{-1}. The measured peak responses show red shifts of larger than 280 cm^{-1} (~35 meV) compared to calculations. A likely reason for this is the effective interface grading due to interface roughness and its effects in the band structure.[35,36] The effective grading results in an effective lowering of the barriers followed by a reduction of the energy spacings.

Since QC detectors operate with zero applied bias, their performance is limited by Johnson noise rather than dark

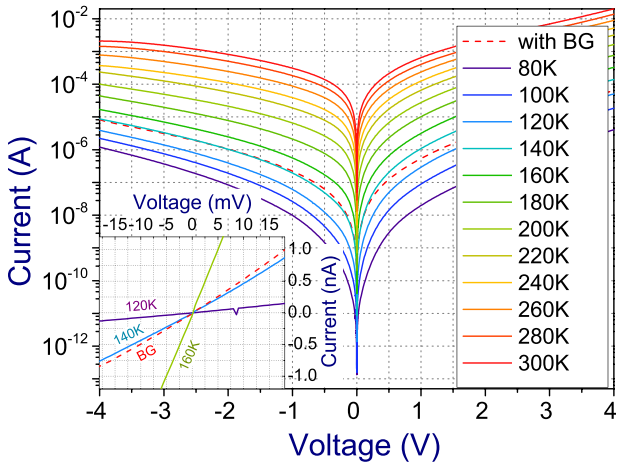

FIG. 3. Solid lines: the dark IV characteristics of design A from 80 K to 300 K, plotted in the semi logarithmic scale. The device size is 0.126 mm^2. Dashed: the IV curve with ambient background illumination (BG) at 80 K. Inset: the dark IV curves near zero bias in linear scale with the BG IV curve, which is close to the dark IV curve at 140 K.

current noise. The Johnson noise can be estimated from the current-voltage (IV) measurements.[9] Dark IV curves with varying temperature are plotted in Fig. 3. At each fixed bias, an exponential increase of the current vs. temperature is observed as expected. The low temperature IV with ambient irradiation (with a field of view of 180 degrees) gives an estimation of background limited infrared performance (BLIP) temperature, which is around 140 K.

The peak current responsivity is $\sim 105\ \mu$A/W for a device with an area of $0.126\,\text{mm}^2$ at BLIP temperature. Light incidence is fixed at the Brewster's angle in the calibration of the responsivity. The total incident light power including the TE and TM components in the open area of the device is used in calculating the responsivity. Detectivity can be calculated with peak responsivity and Johnson noise characteristics and is $\sim 1 \times 10^8$ Jones at the BLIP temperature of 140 K.

As a comparison, we have also investigated the "reversed structure," reversing the growth sequence of the layers of the original design. The calculated band structure is shown in Fig. 4 which also operates as a QC detector. Since both growths are Ga-polarity, the natural biasing of the extraction states from the polarization fields remain in the same direction in both designs, which is clearly seen in Figs. 1 and 4. The calculated optical transition wavelength is the same as the original structure, $\sim 3.6\ \mu$m, with a dipole matrix element of 4.4 Å. However, in the reversed structure, the energy spacings between u and e_2 and between l and e_7 are 55 meV and 30 meV, respectively, considerably smaller than those of the original structure.

The photocurrent spectrum of the reversed structure is also shown in Fig. 2, with a 10 fold lower signal to noise ratio compared to that of the original structure. Also, a second "shoulder" peak at $1800\,\text{cm}^{-1}$ (220 meV) is observed. The peak energy is $\sim$20% less than that of the main transition at around $2300\,\text{cm}^{-1}$ (285 meV). This side peak can be explained by the $l \rightarrow e_2$ optical transition in the reversed structure, which has a dipole matrix element of $z^{rs}_{l,e_2} = 1.9$ Å, 44% of the main optical transition $z^{rs}_{u,l} = 4.4$ Å, and 16% less transition energy. As a comparison, in the original structure $z^{os}_{l,e_2} = 1.1$ Å, only 19% of $z^{os}_{l,u} = 5.7$ Å, with 14% less transition energy. The reversed structure produces a peak responsivity of $\sim 35\ \mu$A/W, with a lower detectivity of 10^4 Jones due to significantly lower resistances.

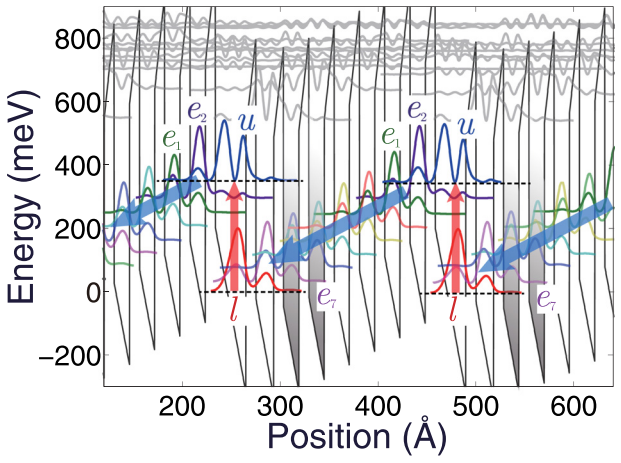

FIG. 4. The reversed QC detector structure with $GaN/Al_{0.5}Ga_{0.5}N$ superlattices. The layer growth sequence of the original design is inverted in the plot, but Si doping of $1.8 \times 10^{18}\,\text{cm}^{-3}$ is still placed in the second and third well to the right of the absorbing well. The optical transition (indicated in the red arrow) is at $\sim 3.6\ \mu$m with a dipole matrix element of 4.4 Å. Growth direction: from left to right.

In conclusion, we have reported the design, fabrication, and characterization of III-nitride QC detectors grown by MOCVD. We have employed only two material compositions in the active layers, i.e., GaN as wells and $Al_0.5Ga_{1-0.5}N$ as barriers. A peak responsivity of $\sim 105\ \mu$A/W for a device with an area of $0.126\,\text{mm}^2$ is recorded, and a detectivity of up to $\sim 1 \times 10^8$ Jones at the BLIP temperature (140 K) is reported. Further optimization of the band structure design and growth calibration are in progress.

This work was supported in part by MIRTHE (NSF-ERC).

[1]H. Schneider and H. Liu, *Quantum well Infrared Photodetectors: Physics and Applications*, Springer Series in Optical Sciences (Springer, 2007).
[2]K. K. Choi, M. D. Jhabvala, J. Sun, C. A. Jhabvala, A. Waczynski, and K. Olver, Appl. Phys. Lett. **103**, 201113 (2013).
[3]A. P. Ravikumar, G. Chen, K. Zhao, Y. Tian, P. Prucnal, M. C. Tamargo, C. F. Gmachl, and A. Shen, Appl. Phys. Lett. **102**, 161107 (2013).
[4]A. V. Barve, T. Rotter, Y. Sharma, S. J. Lee, S. K. Noh, and S. Krishna, Appl. Phys. Lett. **97**, 061105 (2010).
[5]P. Rauter, G. Mussler, D. Grützmacher, and T. Fromherz, Appl. Phys. Lett. **98**, 211106 (2011).
[6]P. Reininger, B. Schwarz, A. Harrer, T. Zederbauer, H. Detz, A. Maxwell Andrews, R. Gansch, W. Schrenk, and G. Strasser, Appl. Phys. Lett. **103**, 241103 (2013).
[7]S.-Q. Zhai, J.-Q. Liu, F.-Q. Liu, and Z.-G. Wang, Appl. Phys. Lett. **100**, 181104 (2012).
[8]J. Yin and R. Paiella, Opt. Express **18**, 1618 (2010).
[9]F. Giorgetta, E. Baumann, M. Graf, Q. Yang, C. Manz, K. Köhler, H. Beere, D. Ritchie, E. Linfield, A. Davies, Y. Fedoryshyn, H. Jäckel, M. Fischer, J. Faist, and D. Hofstetter, IEEE J. Quantum Electron. **45**, 1039 (2009).
[10]D. Hofstetter, M. Beck, and J. Faist, Appl. Phys. Lett. **81**, 2683 (2002).
[11]F. F. Sudradjat, W. Zhang, J. Woodward, H. Durmaz, T. D. Moustakas, and R. Paiella, Appl. Phys. Lett. **100**, 241113 (2012).
[12]A. Pesach, E. Gross, C.-Y. Huang, Y.-D. Lin, A. Vardi, S. E. Schacham, S. Nakamura, and G. Bahir, Appl. Phys. Lett. **103**, 022110 (2013).
[13]M. Beeler, E. Trichas, and E. Monroy, Semicond. Sci. Technol. **28**, 074022 (2013).
[14]B. Sherliker, M. Halsall, I. Kasalynas, D. Seliuta, G. Valusis, M. Vengris, M. Barkauskas, V. Sirutkaitis, P. Harrison, V. D. Jovanovic, D. Indjin, Z. Ikonic, P. J. Parbrook, T. Wang, and P. D. Buckle, Semicond. Sci. Technol. **22**, 1240 (2007).
[15]D. Hofstetter, S.-S. Schad, H. Wu, W. J. Schaff, and L. F. Eastman, Appl. Phys. Lett. **83**, 572 (2003).
[16]A. Vardi, S. Sakr, J. Mangeney, P. K. Kandaswamy, E. Monroy, M. Tchernycheva, S. E. Schacham, F. H. Julien, and G. Bahir, Appl. Phys. Lett. **99**, 202111 (2011).
[17]F. F. Sudradjat, W. Zhang, K. Driscoll, Y. Liao, A. Bhattacharyya, C. Thomidis, L. Zhou, D. J. Smith, T. D. Moustakas, and R. Paiella, Phys. Status Solidi C **9**, 588 (2012).
[18]W. Terashima and H. Hirayama, Proc. SPIE **8625**, 862516 (2013).
[19]D. Feezell, Y. Sharma, and S. Krishna, J. Appl. Phys. **113**, 133103 (2013).
[20]C. Edmunds, L. Tang, M. Cervantes, M. Shirazi-HD, J. Shao, A. Grier, A. Valavanis, J. D. Cooper, D. Li, G. Gardner, D. N. Zakharov, Z. Ikonić, D. Indjin, P. Harrison, M. J. Manfra, and O. Malis, Phys. Rev. B **88**, 235306 (2013).
[21]M. Razeghi, IEEE Photon. J. **3**, 263 (2011).
[22]J.-S. Yang, H. Sodabanlu, M. Sugiyama, Y. Nakano, and Y. Shimogaki, Appl. Phys. Lett. **95**, 162111 (2009).
[23]S. Sakr, P. Crozat, D. Gacemi, Y. Kotsar, A. Pesach, P. Quach, N. Isac, M. Tchernycheva, L. Vivien, G. Bahir, E. Monroy, and F. H. Julien, Appl. Phys. Lett. **102**, 011135 (2013).
[24]S. Gryshchenko, M. Klymenko, O. Shulika, I. Sukhoivanov, and V. Lysak, Superlattices Microstruct. **52**, 894 (2012).

[25]S. Sakr, E. Giraud, A. Dussaigne, M. Tchernycheva, N. Grandjean, and F. H. Julien, Appl. Phys. Lett. **100**, 181103 (2012).
[26]A. Vardi, G. Bahir, F. Guillot, C. Bougerol, E. Monroy, S. E. Schacham, M. Tchernycheva, and F. H. Julien, Appl. Phys. Lett. **92**, 011112 (2008).
[27]S. L. Chuang and C. S. Chang, Phys. Rev. B **54**, 2491 (1996).
[28]M. Sugawara, N. Okazaki, T. Fujii, and S. Yamazaki, Phys. Rev. B **48**, 8102 (1993).
[29]G. Bastard, J. Brum, and R. Ferreira, in *Semiconductor Heterostructures and Nanostructures*, Solid State Physics, Vol. 44, edited by H. Ehrenreich and D. Turnbull (Academic Press, 1991), pp. 229–415.
[30]M. Tchernycheva, L. Nevou, L. Vivien, F. Julien, P. Kandaswamy, E. Monroy, A. Vardi, and G. Bahir, Phys. Status Solidi B **247**, 1622 (2010).
[31]H. Morkoç, "Electronic band structure and polarization effects," in *Handbook of Nitride Semiconductors and Devices* (Wiley-VCH Verlag GmbH & Co. KGaA, 2009), pp. 131–321.
[32]I. Vurgaftman, J. R. Meyer, and L. R. Ram-Mohan, J. Appl. Phys. **89**, 5815 (2001).
[33]M. Feneberg and K. Thonke, J. Phys.: Condens. Matter **19**, 403201 (2007).
[34]F. Bernardini and V. Fiorentini, Phys. Rev. B **64**, 085207 (2001).
[35]Y. Song, R. Bhat, C.-E. Zah, and C. Gmachl, in APS March Meeting (2014), Vol. 59.
[36]Y. Song, R. Bhat, P. Bouzi, C.-E. Zah, and C. Gmachl, "Three Dimensional Interface Roughness in Thin Layered Semiconductor Structures and Its Effects on Intersubband Transitions," Phys. Rev. Lett. (submitted).